



Full Text View

[Volume 30, Issue 6 \(June 2000\)](#)

Journal of Physical Oceanography

Article: pp. 1450–1460 | [Abstract](#) | [PDF \(446K\)](#)Upper-Layer Circulation in the South China Sea^{*}

Tangdong Qu

International Pacific Research Center[±], SOEST, University of Hawaii at Manoa, Honolulu, Hawaii

(Manuscript received January 6, 1999, in final form December 15, 1999)

DOI: 10.1175/1520-0485(2000)030<1450:ULCITS>2.0.CO;2

ABSTRACT

Upper-layer circulation is investigated by using all available historical temperature profiles combined with climatological temperature–salinity relationships in the South China Sea. Two cyclonic eddies are revealed: one is located east of Vietnam (called the East Vietnam eddy) and the other is off northwest Luzon (called the West Luzon eddy). Both local Ekman pumping and remotely forced basin-scale circulation are important mechanisms controlling these two eddies. The Luzon Strait transport (relative to 400 db) is estimated to be of the order 3.0 Sv ($1 \text{ Sv} = 1 \times 10^6 \text{ m}^3 \text{ s}^{-1}$) in the mean, and has a seasonal cycle dominated by the annual signal, with a maximum (5.3 Sv) in January–February and a minimum (0.2 Sv) in June–July. Pressure gradients are also examined to explore the dynamics of the intrusion of waters from the Pacific into the South China Sea through the Luzon Strait.

1. Introduction


The South China Sea is the largest marginal sea in the Southeast Asian waters. It connects in the south with the Sulu and Java Seas through a number of shallow passages and in the north with the Pacific Ocean through the deep Luzon Strait ([Fig. 1a](#) ). Based on early hydrographic observations, sea level records, and ship drifts, [Wyrтки \(1961\)](#) provided the first picture of the circulation in the South China Sea that contains basically a cyclonic gyre in winter and an anticyclonic gyre in summer, as a result of the seasonally reversing monsoon. Basin-scale models of the South China Sea have successfully reproduced this circulation pattern and shown many interesting features of the western boundary currents. Among others, [Shaw and Chao \(1994\)](#) demonstrated that the southward jet in winter follows throughout the western boundary, but the northward jet in summer moves away from the coast of Vietnam at about 12°N . In addition, extending the model from seasonal to interannual timescale, recent simulations ([Chao et al. 1996](#); [Wu et al. 1998](#)) also revealed coherence between the circulation of the South China Sea and El Niño–Southern Oscillation (ENSO).

Table of Contents:

- [Introduction](#)
- [Data and methods of analysis](#)
- [Mean state](#)
- [Seasonal variation](#)
- [Forcing mechanisms](#)
- [Summary](#)
- [REFERENCES](#)
- [FIGURES](#)

Options:

- [Create Reference](#)
- [Email this Article](#)
- [Add to MyArchive](#)
- [Search AMS Glossary](#)

Search CrossRef for:

- [Articles Citing This Article](#)


Search Google Scholar for:

- [Tangdong Qu](#)

The basin-scale models, however, neglected, at least downplayed, the interaction of the South China Sea with its surrounding waters by closing all the shallow passages in the Sulu and Java Seas and fixing the depth-integrated transport in the Luzon Strait to [Wyrki's \(1961\)](#) bimonthly estimates. [Metzger and Hurlburt \(1996\)](#) recently carried out a series numerical experiments with a global model domain, and noted the existence of a circulation around the Philippines that involves a westward flow in the Luzon Strait, a southward flow in the Sulu archipelago, and an eastward flow in the Celebes Sea. Further, they suggested that this circulation is primarily a function of large-scale forcing over the Pacific and model geometry; the local monsoon has little effect. But, no observational evidence has been published.

So far, the only observational source referring to the circulation of the South China Sea is the atlases prepared by [Wyrki \(1961\)](#), dating back to about four decades ago. Considering that a lot of data have been available since then, it seems desirable to provide a more accurate description of the South China Sea circulation. The existing hydrographic data coverage is not good enough to resolve the detailed structure of the circulation, in particular those related to the narrow western boundary currents ([Qu et al. 2000](#)). This study utilizes all the available temperature profiles (mainly bottle data and XBT measurements) that outnumber the hydrographic data by about an order. Following [Meyers et al. \(1995\)](#), these temperature profiles, along with the climatological temperature–salinity relationships from [Levitus \(1982\)](#), can be converted to dynamic heights. Maps of dynamic height are presented in the following sections to show the upper-layer circulation of the South China Sea.

2. Data and methods of analysis



Temperature profiles at observed levels recorded on the CD-ROMs of the *World Ocean Atlas 1994* of NOAA/NESDIS/NODC within the region enclosed by the 100-m isobath in the South China Sea (3°–25°N, 105°–120°E) and in the northern Philippine Sea (15°–25°N, 120°–125°E) are used for this study ([Fig. 1b](#) ). The primary procedure for quality control of these data includes removal of profiles with obviously erroneous records and profiles that do not match the characteristics of their surroundings ([Qu et al. 1999](#)). After all the necessary editing processes, the dataset provides 51 510 temperature profiles extending to 100 m or deeper in the region studied. The temporal and spatial distribution of the data is irregular. In time, they spanned the period from the 1920s to the beginning of the 1990s, with a heavily sampled period in 1965–75; no obvious bias in the density of sampling was apparent toward any month of the year. In space, the upper ocean was best sampled in the northern South China Sea, basically north of the line from 7°N, 109°E to 13°N, 120°E, but lacks enough samples to gain a meaningful insight to the south.

Temperatures are averaged along pressure surfaces and converted to dynamic heights in a $0.5^\circ \times 0.5^\circ$ grid by using the [Levitus \(1982\)](#) climatological temperature–salinity relationships. Two smoothing processes are applied. First, we use a three-month-running average, that is, monthly mean temperature is derived from observations in three overlapping months (January–February–March, February–March–April, etc.). Second, we choose variable horizontal radius to include at least five deep (≥ 400 m) observations at each grid. The mean dynamic height fields are finally smoothed using Gaussian filter with an e -folding scale of about 150 km.

The standard deviations (STD) in the monthly dynamic height fields are generally large as a result of interannual and mesoscale variabilities and possibly the uncertainties in the data as well. The typical values of the STDs are 6.0 dyn cm at the surface and 3.5 dyn cm at 100 m. The standard errors, defined as the STDs divided by the square root of the number of measurements ([Meyers et al. 1995](#)), are smaller usually by a factor of three, based typically on 10 deep (>400 m) measurements at each grid.

3. Mean state

a. Dynamic height

The level of no motion is chosen at 400 db, the greatest common depth of the deep-sea observations, or at the bottom of the ocean where water depth is shallower. According to [Wyrki \(1961\)](#), the flow in the Luzon Strait changes sign at about 300 m in winter and about 400 m in summer. So, we feel that this choice of reference level should be reasonable for investigating the upper-layer circulation. Dynamic heights relative to 400 db are calculated from the monthly mean temperature profiles, and these values are then averaged to produce the annual mean values. [Figure 2a](#)  illustrates the annual mean dynamic height at 100 m. It contains basically a large cyclonic gyre north of the line roughly from 10°N, 110°E to 15°N, 120°E. This large cyclonic gyre has two cores (<65 dyn cm). One is located west of Luzon (called West Luzon eddy below) and other is off east Vietnam (called the East Vietnam eddy below). As can be seen in the following sections, the existence of these two eddies is an essential element of the upper-layer circulation in the northern South China Sea. Circulation in the southern South China Sea, namely south of the line from 10°N, 110°E to 15°N, 120°E, is generally weak. Poor data coverage ([Fig. 1b](#) ) there does not allow further investigation.

The STD of monthly dynamic heights from the annual mean value is also obtained during the averaging. At 100 m, it (Fig. 2b) consists of two major features. One is a high variability core (>2.5 dyn cm) off Luzon. The other is a low variability belt (<1.0 dyn cm) along the continental slope south of China, roughly following the intrusion path of the North Pacific waters (Qu et al. 2000). The former apparently represents the large seasonal variability of the West Luzon eddy, while the latter could be interpreted as evidence that the seasonally reversing monsoon has less effect on the intrusion current than on the local circulation.

b. Transport

Annual mean depth-integrated dynamic height is presented in Fig. 3a to show the volume transport of the upper-layer circulation in the South China Sea. Given the depth-integrated dynamic heights P_E at station E and P_F at station F , the volume transport between these two stations, Q_{EF} , can be obtained by

$$Q_{EF} = (P_E - P_F)g/f,$$

where g is the acceleration due to gravity and f is the Coriolis parameter.

In the center of the large cyclonic gyre of the northern South China Sea, depth-integrated dynamic height is depressed by about 10 m^2 (Fig. 3a). On the assumption of geostrophy, this depression implies a basin-scale circulation of the order 4 Sv. In the Luzon Strait, contours of depth-integrated dynamic height slope slightly toward the west on the northern side, indicative of a westward intrusion of waters from the Pacific into the South China Sea, commonly referred to as the Luzon Strait transport (Wyrski 1961; Nitani 1972). But, its strength is rather weak compared with the northward flow (the Kuroshio).

The estimate of the Luzon Strait transport is sensitive to the selection of the cross section, because the property gradient in the zonal direction is much greater than that in the meridional direction and so the signal of the intrusion current might be contaminated by the fluctuation of the Kuroshio. According to earlier studies (e.g., Wyrski 1961; Nitani 1972), however, much of the Kuroshio returns to the Pacific before reaching 121°E in the Luzon Strait. As such, the effect of the Kuroshio is expected to be less important to the west of that longitude. We chose a cross section along the western edge of the strait, with its northern end (station A, 120°E) at the continental slope southwest of Taiwan and its southern end (station B, 120.5°E) at the continental slope northwest of Luzon (Fig. 1a). Depth-integrated dynamic heights at these two stations are obtained by averaging the data within their respective $0.5^\circ \times 0.5^\circ$ bins. No further spatial smoothing is applied. The difference of depth-integrated dynamic height (15.2 m^2) between stations A and B yields a transport estimate of 3.0 Sv through the Luzon Strait. Directly wind-driven Ekman transport is relatively weak (about 0.3 Sv), accounting for only about 10% of the geostrophic component.

The STD of monthly depth-integrated dynamic heights from the annual mean value (Fig. 3b) demonstrates essentially the same pattern as those of Fig. 2b, with its largest amplitude coinciding with the West Luzon eddy and its lowest amplitude along the continental slope south of China. The details of these variabilities are investigated below.

4. Seasonal variation

The seasonal variation of dynamic height at 100 m (Fig. 4) is dominated by the growth and decay of two cyclonic eddies—the West Luzon eddy and the East Vietnam eddy. The West Luzon eddy is about several hundred kilometers offshore between 17° and 19°N northwest of Luzon. It first appears in November, reaches its maximum strength in January–February, and decays after May–June. The East Vietnam eddy, featured by a narrow belt of low dynamic height east of Vietnam, is present in summer (June–August), and tends to strengthen toward the end of the season when prevailing wind is from the southwest (October–November). Interestingly, this cyclonic circulation continues to exist in winter, until the transition of monsoon from the northeast to the southwest (March–May).

The existence of the West Luzon eddy in winter and East Vietnam eddy in summer has been reported, though differently described, by several earlier studies (cf. Chu et al. 1998). Among others, Shaw et al. (1996) referred to the West Luzon eddy as a major upwelling region northwest of Luzon, whereas He et al. (1996) called both of them mesoscale cyclonic circulation. Recent satellite altimeter data also provided evidence on the alternative appearance of these two eddies. According to Shaw et al. (1999), sea level off Luzon has largest positive anomaly in August and largest negative anomaly in December. Annual oscillation of sea level was also observed off Vietnam, but the extreme positive and negative anomalies are in April and October, respectively. The seasonal variation of dynamic height shown in Fig. 4 is basically consistent with Shaw et al.'s results. But, we found that there is no anticyclonic circulation west of Luzon in August, and the East Vietnam eddy appears to exist even in winter when the prevailing wind is from the northeast. One obvious reason for this difference is that hydrographic data include the annual mean field of dynamic height but satellite altimeter data do not.

Notice that the western boundary current is not well resolved in [Fig. 4](#), presumably as a result of smoothing. In particular, as northeastward flow exists over a large part of the basin in summer, the narrow western boundary current is almost smoothed away. However, careful examination of the dynamic topography indicates that there is a southwestward pressure gradient along the continental slope south of China during all seasons of the year. This pressure gradient likely provides the pressure head driving a western boundary current against friction ([Chao et al. 1996](#); [Qu et al. 1998](#)). We will return to this point in [section 5c](#).

5. Forcing mechanisms

a. Local wind

The seasonal forcing in the South China Sea is dominated by two monsoons, summer and winter, every year. To see the response of the upper-layer circulation to the monsoonal wind, maps of wind stress curl and its seasonal variability from [Hellerman and Rosenstein's \(1983\)](#) monthly climatology are presented. The annual mean wind stress curl ([Fig. 5a](#)) has a dipole pattern: anticyclonic curl in the north and cyclonic curl in the south, with the zero wind stress curl line roughly located from about 15°N, 110°E to 20°N, 120°E. The maximum wind stress curl ($>20 \times 10^{-8} \text{ N m}^{-3}$) is seen at the center of the West Luzon eddy. Near the coast of Vietnam, wind stress curl is also positive, but its magnitude (about $5 \times 10^{-8} \text{ N m}^{-3}$) is much less than that to the east.

The STD of monthly wind stress curls from the annual mean value ([Fig. 5b](#)) provides information on the strength of seasonal variability. In addition to the large STDs ($>15 \times 10^{-8} \text{ N m}^{-3}$) corresponding to the positive and negative mean wind stress curl cores, high variability ($>20 \times 10^{-8} \text{ N m}^{-3}$) is also seen southeast of Vietnam. Interestingly, despite higher variability of wind stress curl, seasonal fluctuation of dynamic height in the East Vietnam eddy is considerably weaker than that in the West Luzon eddy ([Figs. 2b](#) and [3b](#)).

Monthly wind stress has a cyclonic curl ($>20 \times 10^{-8} \text{ N m}^{-3}$) or, equivalently, an upward Ekman pumping ($>1 \times 10^{-5} \text{ m s}^{-1}$) centered at the West Luzon eddy from October through April, with a maximum strength exceeding $50 \times 10^{-8} \text{ N m}^{-3}$ in December ([Fig. 6](#)). This cyclonic wind stress curl decays during the rest of the year, in phase with the West Luzon eddy. As upwelling (the West Luzon eddy) was observed at about 100 km offshore and not at the coast, despite the prevailing coastal, upwelling-favorable northeasterly wind in winter, [Shaw et al. \(1996\)](#) speculated that it is not driven by coastal wind but arisen from remotely forced basin-wide circulation. We emphasize that wind stress curl or direct Ekman pumping may play a major role in generating the West Luzon eddy.

Wind stress curl varies dramatically near the coast of Vietnam, featured by an anticyclonic curl from November to April and a cyclonic curl from May to October ([Fig. 6](#)), both having a maximum exceeding $30 \times 10^{-8} \text{ N m}^{-3}$ in magnitude. The presence of the East Vietnam eddy can be explained at least partly by wind stress curl from late summer to early fall but not in winter, indicative of strong influence of remotely forced processes. During the northeast monsoon season, the northeast-to-southwest oriented zero wind stress curl line separates the South China Sea into two parts ([Fig. 6](#)). In the northwest, the northeasterly wind produces shoreward Ekman current. Owing to the constraint of zero transport on the shore, water is accumulated against the coast, and as a result a cross-shelf pressure gradient is set up, which eventually generates a southwestward flow via geostrophy (cf. [Qu et al. 1998](#)). On the other hand, the piling up of water also produces high sea level southwest of Vietnam, as has already been described in literature (e.g., [Wyrтки 1961](#); [Shaw and Chao 1994](#); [Chao et al. 1996](#)). The high sea level southwest of Vietnam produces an opposite directed pressure gradient that prevents the western boundary current from flowing to the farther south but turning eastward off Vietnam.

In summary, the formation of a gyre, whatever cyclonic or anticyclonic, seems to be better determined by wind stress curl in the eastern part than in the western part of the basin, reflecting the westward intensification induced by β -effect ([Wyrтки 1961](#); [Chao et al. 1996](#); [Chu et al. 1998](#)). Consequently, the remotely forced basin-scale circulation is likely to play a more important role in the formation of the East Vietnam eddy than in the formation of the West Luzon eddy.

b. Pressure gradient across the Luzon Strait

Pressure gradient across the Luzon Strait, regarded as the dynamic height difference between stations A and B ([Fig. 1a](#)), determines the Luzon Strait transport ([section 3b](#)). Surface heat flux and the piling up of water forced by monsoonal wind might be the important mechanisms that maintain and change this pressure gradient.

In winter, intense atmospheric cooling ($<-200 \text{ W m}^{-2}$; [Oberhuber 1988](#)) reduces the upper ocean temperature and sets down the sea level in the Luzon Strait. On the other hand, surface water is forced by northeast wind to flow against the coast of Taiwan, and this will set up the sea level at station A ([Fig. 7a](#)). This condition is just reversed in summer. The

large degree of cancellation between the effects of surface heat flux and wind stress induces lower sea level from January through June and higher sea level during the rest of the year at station A, with its minimum in March–April and maximum in September–October. For some unclear reasons the seasonal cycle tends to lag behind in deeper layers, indicative of a signal of downward propagation. On the southern side of the strait (station B), the effects of surface heat flux and wind stress have the same phase, both producing higher sea level in summer and lower sea level in winter (Fig. 7b).

The seasonal variation of depth-integrated dynamic height difference between stations A and B (Fig. 8a) shows a strong annual signal, with its minimum of 1.0 m^2 in June–July and maximum of 26.2 m^2 in January–February. In the latitude of 20°N , this result implies that the Luzon Strait transport has a minimum transport of 0.2 Sv and a maximum transport of 5.3 Sv in June–July and January–February, respectively. Although directly wind driven circulation does not appear to make a significant contribution to the Luzon Strait transport, the piling up of water induced by wind stress might be an important mechanism changing the pressure gradient that eventually determines that transport.

c. Pressure gradient along the continental slope south of China

Qu et al. (2000) revealed that the intrusion of the high salinity water from the Pacific into the South China Sea contains a pronounced semiannual signal. In particular, the intrusion has a stronger strength in summer than prior to and after it, despite the prevailing southwest monsoon. Apparently, this semiannual signal cannot be explained by the pressure gradient across the Luzon strait (Fig. 8a).

Before investigating this problem further, it must be noted that there is an essential difference between the intrusion strength referred to by Qu et al. (2000) and the Luzon Strait transport discussed here. The former is inferred from water property distributions, and is well defined as a narrow western boundary current along the continental slope south of China. The latter, however, is a measure of the net transport through the Luzon Strait, a function of the inflow of the North Pacific waters and the outflow of the South China Sea waters as well. For this concern, it might be useful to examine the pressure gradient along the continental slope south of China in order to understand the dynamics of the intrusion.

In a sense of liner dynamics, the intrusion current along the continental slope south of China is primarily controlled by the following equations (Godfrey 1989; Qu et al. 1998):

$$fv = -\frac{1}{\rho} \frac{\partial p}{\partial x}, \quad (1)$$

$$-fu = -\frac{1}{\rho} \frac{\partial p}{\partial y} + F_y, \quad (2)$$

where $\rho^{-1} \partial p / \partial x$ represents the cross-shelf pressure gradient, $\rho^{-1} \partial p / \partial y$ is the longshore pressure gradient, and F_y denotes the friction along the continental slope south of China. On one hand, the intrusion current is geostrophic and can be well determined by the cross-shelf pressure gradient [Eq. (1)]; on the other hand, longshore pressure gradient provides the pressure head driving the current against friction [Eq. (2)]. On the longshore average, the pressure gradient along the continental slope south of China can be regarded as the dynamic height difference between stations A and C (Fig. 1a). We use these two stations to infer this basinwide longshore pressure gradient, simply because they represent the starting and ending points of the intrusion current, respectively. The stations can also be chosen elsewhere at the western boundary, provided the question of how these stations are representative is born in mind, but the results are qualitatively insensitive to the selection of the stations (not shown).

The depth-integrated dynamic height at station A is about 16.1 m^2 higher than that at station C in the mean (also see Fig. 3a). Its seasonal variation shows a semi-annual signal of comparable strength with the annual cycle at station C (Fig. 7c), but of only about $1/3$ in amplitude of the annual cycle at station A (Fig. 7a). Another interesting result is that the dynamic height at station C reaches its seasonal minimum in summer, despite intense surface heating ($>50 \text{ W m}^{-2}$; Oberhuber 1988). The low sea level off Vietnam in summer has been reported by several earlier studies (e.g., Wyrski 1961; Shaw and Chao 1994; Chao et al. 1996), mainly as a result of southwest monsoon. The shoreward Ekman transport forced by northeasterly wind produces high sea level in winter.

The seasonal variation of dynamic height difference between stations A and C contains a semiannual signal of comparable strength with that of annual signal (8.5 vs 7.4 m^2), with maxima in August and February and minima in April and November (Fig. 8b). Surprisingly, this semiannual signal shows essentially the same phase as the intrusion strength inferred from water mass distribution (Qu et al. 2000). It seems preferable to suggest that longshore pressure gradient is the primary

mechanism driving the intrusion current against friction at the continental slope south of China [Eq. (2)]. However, one must keep in mind that nonlinear effects (e.g., the advective terms in the momentum equations) could also be important in the intrusion process. This has to be investigated further by research.

6. Summary

Two cyclonic eddies, namely, the West Luzon eddy and the East Vietnam eddy, are revealed in the upper layers of the South China Sea. The West Luzon eddy exists at about 18°N, 118°E from late fall to early spring, coinciding surprisingly well with a positive wind stress curl both in location and time. The East Vietnam eddy, located at about 14°N, 110°E, is seen from late summer to early fall, when local Ekman pumping is positive, but also in winter, when local Ekman pumping is negative. Dynamical consideration suggests that both local wind stress curl and basin-scale circulation are important in the formation of these eddies. But the relative importance between them seems to decrease toward the west.

The existence of the two cyclonic eddies provides the basis for describing the upper-layer circulation in the South China Sea. In winter, as both eddies are developed, a basin-wide cyclonic gyre exists over the northern basin. In summer, northeastward flow becomes widely spread as a result of the prevailing southwest monsoon, but there is still some indication that a narrow western boundary current flows in the opposite direction along the continental slope south of China. Circulation in the southern South China Sea is relatively weak. Poor data coverage there does not permit further investigation.

Despite some uncertainty due to the effect of the Kuroshio, the annual mean Luzon Strait transport relative to 400 db is estimated to be of the order 3 Sv. Directly wind driven Ekman transport is small (0.3 Sv), accounting for only about 10% of the geostrophic component. These values are consistent with the earlier estimates provided by [Metzger and Hurlburt \(1996\)](#) and [Qu et al. \(2000\)](#). The seasonal variation of the Luzon Strait transport is dominated by the annual signal, with a maximum (about 5.3 Sv) in January–February and a minimum (about 0.2 Sv) in June–July.

The pressure gradient across the Luzon Strait is strongest in winter, dropping to near zero in summer. This southward push is geostrophically rotated to the westward Luzon Strait transport. Although directly wind-driven Ekman drift has little effect on the mean Luzon Strait transport ([Metzger and Hurlburt 1996](#)), the piling up of water created by monsoonal wind stress is likely to be an important mechanism determining the seasonal fluctuation of the pressure gradient across the Luzon Strait.

The pressure gradient along the continental slope south of China involves a pronounced semiannual signal, with maxima in summer and winter and minima in spring and fall. This seasonal cycle shows a remarkable agreement in phase with the intrusion strength inferred from water mass distribution, and thus might be interpreted as evidence to explain why the intrusion has a stronger strength in summer than prior to and after it ([Qu et al. 2000](#)). In the sense of linear dynamics, this seems to suggest that longshore pressure gradient is the primary mechanism driving the intrusion current along the continental slope south of China.

Finally, we note that in the limitation of XBT measurements the present analysis was restricted only to the upper 400 m. As such, we fail to resolve the previously observed two-layer structure that waters in the salinity maximum (around 130 m) and minimum (around 500 m) layers flow in the opposite direction ([Wyrtki 1961](#); [Qu et al. 2000](#)). Information on deeper currents and better reference levels are further required. A study using the results from general circulation models is under way.

Acknowledgments

This research was funded by Frontier Research System for Global Change. The author is grateful to H. Mitsudera and T. Yamagata for their constant encouragement and advice and to G. Meyers, J. P. McCreary, K. Hanawa, and S. K. Behera for many valuable discussions throughout this study. Thanks are also extended to D. Henderson and two anonymous reviewers for their useful comments and, especially, to N. Hogg for his thoughtful suggestions on the earlier manuscript.

REFERENCES

- Chao, S.-Y., P.-T. Shaw, and S. Y. Wu, 1996: El Nino modulation of the South China Sea circulation. *Progress in Oceanography*, Vol. 38, Pergamon, 51–93.
- Chu, P. C., Y. Chen, and S. Lu, 1998: Wind-driven South China Sea deep basin warm-core/cool core eddies. *J. Oceanogr.*, **54**, 347–360.
- Godfrey, J. S., 1989: A Sverdrup model of the depth-integrated flow for the world ocean allowing for island circulations. *Geophys.*

He, Y., C. Guan, and H. Gao, 1996: Water temperature and circulation structure in the upper ocean of the northern South China Sea (in Chinese). *Acta Oceanol. Sinica*, **6**, 60–69..

Hellerman, S., and M. Rosenstein, 1983: Normal monthly wind stress over the world Ocean with error estimates. *J. Phys. Oceanogr.*, **13**, 1093–1104.. [Find this article online](#)

Levitus, S., 1982: *Climatological Atlas of the World Oceans*. NOAA Prof. Paper No. 13. U.S. Govt. Printing Office, 173 pp..

Metzger, E. J., and H. E. Hurlburt, 1996: Coupled dynamics of the South China Sea, the Sulu Sea, and the Pacific Ocean. *J. Geophys. Res.*, **101**, 12 331–12 352..

Meyers, G., R. J. Bailey, and A. P. Worby, 1995: Geostrophic transport of Indonesian Throughflow. *Deep-Sea Res.*, **42**, 1163–1174..

Nitani, H., 1972: Beginning of the Kuroshio. *Kuroshio: Its Physical Aspects of the Japan Current*, H. Stommel and K. Yoshida, Eds., University of Washington Press, 129–163..

Oberhuber, J. M., 1988: An atlas based on the “COADS” data set: The budgets of heat, buoyancy and turbulent kinetic energy at the surface of the global ocean. Max-Planck-Institut für Meteorologie Rep. 15. [Available from Max-Planck-Institut für Meteorologie, Bundesstrasse 55, D-20146 Hamburg, Germany..]

Qu, T., H. Mitsudera, and T. Yamagata, 1998: On the western boundary currents in the Philippine Sea. *J. Geophys. Res.*, **103**, 7537–7548..

—, —, and —, 1999: A climatology of the circulation and water mass distribution near the Philippine coast. *J. Phys. Oceanogr.*, **29**, 1488–1505..

—, —, and —, 2000: The intrusion of the North Pacific waters into the South China Sea. *J. Geophys. Res.*, **105**, 6415–6424..

Shaw, P.-T., and S.-Y. Chao, 1994: Surface circulation in the South China Sea. *Deep-Sea Res.*, **41**, 1663–1683..

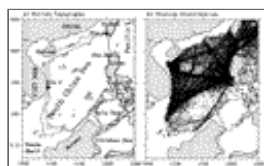
—, —, K.-K. Liu, S.-C. Pai, and C. T. Liu, 1996: Winter upwelling off Luzon in the northeast South China Sea. *J. Geophys. Res.*, **101**, 16 435–16 448..

—, —, and L.-L. Fu, 1999: Sea surface height variations in the South China Sea from satellite altimetry. *Oceanol. Acta*, **22**, 1–17..

Wu, C.-R., P.-T. Shaw, and S.-Y. Chao, 1998: Seasonal and interannual variations in the velocity field of the South China Sea. *J. Oceanogr.*, **54**, 361–372..

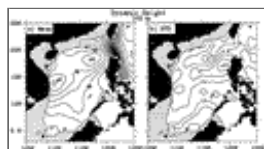
Wyrtki, K., 1961: Physical oceanography of the Southeast Asian waters. Naga Rep. 2, 195 pp. [Available from Scripps Institution of Oceanography, University of California, San Diego, La Jolla, CA 92093..]

Figures



[Click on thumbnail for full-sized image.](#)

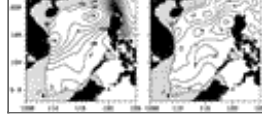
Fig. 1. (a) Bottom topography and (b) station distribution in the South China Sea.



[Click on thumbnail for full-sized image.](#)

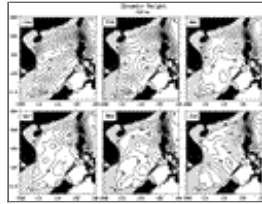
Fig. 2. (a) Annual mean and (b) standard deviation (STD) of dynamic height (dyn cm) at 100 m (relative to 400 db). Contour intervals are 1 dyn cm in (a) and 0.5 dyn cm in (b). Region with water depth shallower than 100 m is stippled.





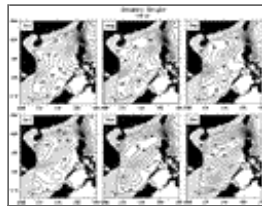
Click on thumbnail for full-sized image.

Fig. 3. Same as [Fig. 2](#) except for depth-integrated (0–400 m) dynamic height (m^2). Contour intervals are 2 m^2 in (a) and 1 m^2 in (b).



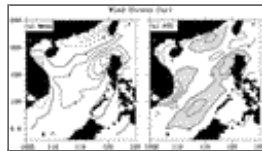
Click on thumbnail for full-sized image.

Fig. 4. Monthly mean dynamic height (dyn cm) at 100 m. Contour interval is 1 dyn cm. Region with water depth shallower than 100 m is stippled.



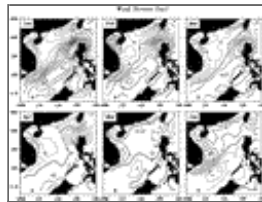
Click on thumbnail for full-sized image.

Fig. 4. (Continued)



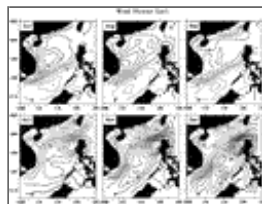
Click on thumbnail for full-sized image.

Fig. 5. (a) Annual mean and (b) standard deviation (STD) of wind stress curl (10^{-8} N m^{-3}) from [Hellerman and Rosenstein \(1983\)](#). Contour interval is $5 \times 10^{-8} \text{ N m}^{-3}$. Region with STD greater than $10 \times 10^{-8} \text{ N m}^{-3}$ is stippled in (b).



Click on thumbnail for full-sized image.

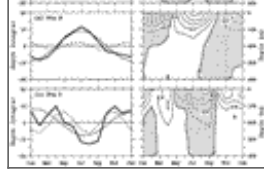
Fig. 6. Monthly mean wind stress curl (10^{-8} N m^{-3}). Contour interval is $5 \times 10^{-8} \text{ N m}^{-3}$.



Click on thumbnail for full-sized image.

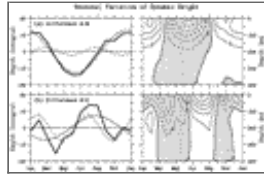
Fig. 6. (Continued)





[Click on thumbnail for full-sized image.](#)

Fig. 7. Seasonal variation of dynamic height (dyn cm, right panels) and its depth integral (m^2 , left panels) at stations (a) A, (b) B, and (c) C. Annual (light solid) and semiannual (light dashed) harmonic fits of depth-integrated dynamic height (heavy solid) are included on the left panels, where the mean values of 198.6, 183.4, and 182.5 m^2 have been subtracted before plotting in (a), (b), and (c), respectively.



[Click on thumbnail for full-sized image.](#)

Fig. 8. Same as [Fig. 7](#) except for the difference (a) between stations A and B and (b) between stations A and C. The mean values of 15.2 and 16.1 m^2 have been subtracted before plotting in (a) and (b), respectively.

* School of Ocean and Earth Science and Technology Contribution Number 4956, and International Pacific Research Center Contribution Number IPRC-29.

+ International Pacific Research Center is partly sponsored by Frontier Research System for Global Change.

Corresponding author address: Dr. Tangdong Qu, IPRC–SOEST, University of Hawaii at Manoa, 2525 Correa Road, Honolulu, HI 96822.

E-mail: tangdong@soest.hawaii.edu

[top](#) ▲



© 2008 American Meteorological Society [Privacy Policy and Disclaimer](#)
 Headquarters: 45 Beacon Street Boston, MA 02108-3693
 DC Office: 1120 G Street, NW, Suite 800 Washington DC, 20005-3826
amsinfo@ametsoc.org Phone: 617-227-2425 Fax: 617-742-8718
[Allen Press, Inc.](#) assists in the online publication of AMS journals.